IV International Conference on Computational Methods for Coupled Problems in Science and Engineering
COUPLED PROBLEMS 2011
M. Papadrakakis, E. Oñate and B. Schrefler (Eds)

FINITE ELEMENT METHOD FOR STRONGLY-COUPLED SYSTEMS OF FLUID-STRUCTURE INTERACTION WITH APPLICATION TO GRANULAR FLOW IN SILOS

SVEN REINSTÄDLER *, ANDREAS ZILIAN * AND DIETER DINKLER *

*Institute for Structural Analysis
TU Braunschweig
Beethovenstr. 51, 38106 Braunschweig, Germany
e-mail: s.reinstaedler@tu-bs.de, www.statik.tu-bs.de

Key words: Thin-walled Structure, Non-Newtonian Fluid, Space-Time Finite Elements, Level-Set-Method, XFEM

Abstract. A monolithic approach to fluid-structure interactions based on the space-time finite element method (STFEM) is presented. The method is applied to the investigation of stress states in silos filled with granular material during discharge. The thin-walled silo-shell is modeled in a continuum approach as elastic solid material, whereas the flowing granular material is described by an enhanced viscoplastic non-Newtonian fluid model. The weak forms of the governing equations are discretized by STFEM for both solid and fluid domain. To adapt the matching mesh nodes of the fluid domain to the structural deformations, a mesh-moving scheme using a neo-Hookean pseudo-solid is applied. The finite element approximation of non-smooth solution characteristics is enhanced by the extended finite element method (XFEM). The proposed methodology is applied to the 4D (space-time) investigation of deformation-dependent loading conditions during silo discharge.

1 MOTIVATION

While the civil engineer of a silo-shell is interested in the pressure affecting the structure, the process engineer must ensure that the granular material discharges as a mass flow. If the funnel-shaped discharge zone is not well-suited for mass flow, consolidated granulars may build inner slots and so-called “dead zones” may occur. In case of kernel flow, which is also provided by an excentric discharge opening, the stress states inside the silo are unknown. If inner slots appear close to the silo wall, the structure is not loaded symmetrically anymore, which may lead to overload and failure.

2 INTRODUCTION

This contribution discusses recent developments in simultaneous (monolithic) analysis of fluid-structure interaction based on the space-time finite element method. A weighted residual-based approach to numerical analysis of fluid flow along flexible thin-walled structures, enabling the investigation of flow-induced vibrations of strongly coupled systems, is presented. Within the simultaneous solution procedure, velocity variables are used for both fluid and solid, and the whole set of model equations is discretized by a stabilized time-discontinuous space-time finite element method (TD-STFEM). The flexible structure is modeled using a three-dimensional continuum approach in a total Lagrangian setting considering large displacements. In the flow domain the incompressible Navier-Stokes equations describe the characteristics of flowing granular material as non-Newtonian fluid. A continuous finite element mesh is applied to the entire spatial domain, and the discretized model equations are assembled in a single set of algebraic equations, considering the two-field problem as a whole. The continuous fluid-structure mesh with identical orders of approximation for both solid and fluid in space and time automatically yields conservation of mass and momentum at the fluid-structure interface. A mesh-moving scheme is used to adapt the nodal coordinates of the fluid space-time finite element mesh to the structural deformation.

3 STRONG FORM OF MODEL EQUATIONS

3.1 Elasto-dynamics of the continuum-based structural model

The state of motion of deformable continua is characterized by displacements $\boldsymbol{u}$ and velocities $\boldsymbol{v} = \dot{\boldsymbol{u}}$. The rate of deformation is described by the nonlinear Green-Lagrangian strain rate tensor $\dot{\boldsymbol{E}} = \frac{1}{2}(\dot{\boldsymbol{F}}^T\boldsymbol{F} + \boldsymbol{F}^T\dot{\boldsymbol{F}})$, where $\boldsymbol{F} = \boldsymbol{I} + \nabla_0\boldsymbol{u}$ denotes the deformation gradient. The balance equation of momentum

$$\rho_0\ (\dot{\boldsymbol{v}} - \boldsymbol{b}) - \nabla_0 \cdot (\boldsymbol{F}\boldsymbol{S}) = \boldsymbol{0} \tag{1}$$

has to be fulfilled in the reference space-time domain $Q_0 = \Omega_0 \times [0, T]$ (subscript 0). ρ_0 indicates structural density and $\rho_0\,\boldsymbol{b}$ the body forces. The material behavior is assumed to be elastic and is described by the second Piola-Kirchhoff stress tensor $\mathbf{S}$, the Green Lagrange strain tensor and the tensor $\mathbb{C}$ of elasticity, which is deduced from the strain-energy function Ψ

$$\dot{\boldsymbol{S}} = \mathbb{C} : \dot{\boldsymbol{E}} \quad \text{with} \quad \mathbb{C} = \frac{\partial^2 \Psi}{\partial^2 \boldsymbol{E}} \tag{2}$$

shown in rate formulation. Close to critical loads, the thin-walled shell structure may be subjected to large deformations at small strains. Therefore, the elasticity tensor of the St. Venant-Kirchhoff model can be applied, which is defined by the strain-energy function $\Psi = \frac{1}{2}\lambda(\mathrm{tr}\boldsymbol{E})^2 + \mu\,\boldsymbol{E} : \boldsymbol{E}$ depending on the Lamé coefficients λ and μ as model parameters.

3.2 Fluid dynamics

The motion of viscous and incompressible fluids is governed by momentum balance and continuity equation

$$\rho\left(\frac{\partial \boldsymbol{v}}{\partial t} + \boldsymbol{v}\cdot\nabla\,\boldsymbol{v} - \boldsymbol{b}\right) - \nabla\cdot\boldsymbol{\sigma} = \mathbf{0} \tag{3}$$

$$\nabla\cdot\boldsymbol{v} = 0 \tag{4}$$

which are defined in the deforming space-time domain $Q = \Omega \times [0,T]$ of the current configuration. The flow characteristics of the granular material is described by a phenomenological material model for incompressible viscoplastic fluids applying a power law as a first approach, where

$$\boldsymbol{\sigma} = -p\,\mathbf{I} + \phi\,\mathbf{D} \quad \text{with} \quad \phi = \frac{p\cdot\sin(\varphi)+c}{\sqrt{J_2^{\mathbf{D}}+\epsilon}} + 2\,\eta\,\left(4\,J_2^{\mathbf{D}}\right)^{\frac{\nu-1}{2}} \tag{5}$$

denotes the Cauchy stress tensor [4]. The viscosity ϕ depends on the pressure p and the second invariant $J_2^{\mathbf{D}}$ of the strain rate tensor $\boldsymbol{D} = \frac{1}{2}\left(\nabla\boldsymbol{v} + (\nabla\boldsymbol{v})^T\right)$, describing the kinematics. The limit state between material at rest and flow is characterized by the angle of friction φ and cohesion c as model parameters. In case of increasing strain rates the mechanical behaviour is further described by a power law, depending on the viscosity η and ν. The regularisation parameter $\epsilon \ll 1$ ensures the evaluation of stress states for disappearing strain rates, see Figure 1 .

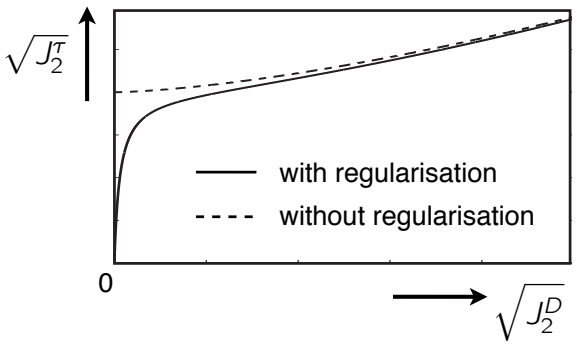

Figure 1: Stress-strain-relation [4]

4 SPACE-TIME WEAK FORM AND DISCRETIZATION

A monolithic approach to fluid-structure interaction is chosen in order to develop an accurate and uniform solution procedure for coupled systems exhibiting strong interactions [3]. The governing equations for both solid and fluid are formulated in terms of velocity variables and are discretized with the TD-STFEM [1]. A continuous finite element mesh is applied to the entire spatial domain, and the discretized model equations are assembled into a single set of algebraic equations, considering the multi-field problem as a whole.

The space-time finite element method provides a consistent discretization of both space and time, avoiding semi-discrete formulations. For the sake of efficiency, the space-time domain Q is subdivided into a sequence of space-time slabs $Q_n = \Omega \times [t_n, t_{n+1}]$ which are solved successively.

4.1 Space-time finite element formulation of geometric nonlinear elastic solids

The TD-STFEM formulation of the geometric nonlinear elastic solid within the time slab $Q_{0,n}$ reads

$$\int_{Q_{0,n}} \delta\boldsymbol{v} \cdot \rho_0 \left(\dot{\boldsymbol{v}} - \boldsymbol{b}\right) dQ_0 + \int_{Q_{0,n}} \dot{\boldsymbol{E}}(\delta\boldsymbol{v}, \boldsymbol{u}) \,:\, \boldsymbol{S}\, dQ_0 \tag{6}$$

$$+ \sum_e \int_{Q_{0,n}} \delta\boldsymbol{S} : \left(\mathbb{C}^{-1} : \dot{\boldsymbol{S}} - \dot{\boldsymbol{E}}(\boldsymbol{v}, \boldsymbol{u})\right) dQ_0 \tag{7}$$

$$+ \int_{\Omega_0} \delta\boldsymbol{v}^T(t_n^+) \cdot \rho_0 \left(\boldsymbol{v}(t_n^+) - \boldsymbol{v}(t_n^-)\right) d\Omega_0 \tag{8}$$

$$+ \sum_e \int_{\Omega_0} \delta\boldsymbol{S}(t_n^+) : \mathbb{C}^{-1} : \left(\boldsymbol{S}(t_n^+) - \boldsymbol{S}(t_n^-)\right) d\Omega_0 \tag{9}$$

$$+ \sum_e \int_{\Omega_0} \boldsymbol{\tau}^S \cdot \delta\dot{\boldsymbol{v}} \cdot \left(\rho_0 \left(\dot{\boldsymbol{v}} - \boldsymbol{b}\right) - \nabla_0 \cdot (\boldsymbol{F}\boldsymbol{S})\right) dQ_0 = 0 \tag{10}$$

where e runs over all elements.

The resulting displacement field $\boldsymbol{u}$ determined by time integration of the velocities and continuous in both space and time, is needed for computing the Green-Lagrange rate of strain tensor $\dot{\boldsymbol{E}}(\boldsymbol{u}, \boldsymbol{v})$ respectively the deformation gradient $\boldsymbol{F}(\boldsymbol{u})$. In the finite element formulation above, line (6) represents the weak form of momentum balance, line (7) fulfills the constitutive law for the state of thermodynamic equilibrium in weighted residual form at element level. The jump terms for velocities in (8) and equilibrium stress in (9) satisfy

the initial conditions of the time slab in integral form. The line (10) represents a Petrov-Galerkin stabilization of the momentum equation with the stabilization parameter

$$\tau_{ij}^{S} = \begin{cases} 0 & i \neq j \\ \frac{1}{\sqrt{\left(\frac{2}{\Delta t}\right)^2 + \left(\frac{2\,c_p}{\Delta x_i}\right)^2}} & i = j \end{cases} \tag{11}$$

following Hughes and Hulbert [1] depending on the time slab width Δt, the velocity $c_p = \sqrt{\frac{\lambda+2\,\mu}{\rho}}$ of compression waves and the characteristic element length Δx_i in the i-th direction.

The Dirichlet boundary condition is fulfilled exactly by the approximation space for the velocity field. While homogenous Neumann boundary condition are fulfilled in weak form, surface loads can be included into the formulation by the integral $\int \delta \boldsymbol{v}\, \boldsymbol{h}_0\, dP_0^N$ over the Neumann boundary P_0^N.

To represent the curvature of thin-walled shell-structures, second order polynomials of the serendipity family are used for geometry description of the finite elements. The same approximation is used for the velocities, which are continuous in space and discontinuous and piecewise linear in time.

In contrast, the ansatz functions for the stresses are discontinuous in both space and time, leading to a mixed-hybrid formulation in which stress variables are defined only inside finite elements. The approximation of the normal stresses is chosen with respect to the constitutive equation, assuming linear kinematics and Poisson's ratio equal to zero. In this case the normal stresses are proportional to the velocity gradient in the appropriate direction ($\sigma_{ii} \approx v_{i,i}$). Thus the approximation is trilinear in the particular direction of the stress component and perpendicular quadratic. To fulfill the LBB condition and suppress numerical phenomena like shear locking the shear stresses are approximated by lower order shape functions. To improve the performance of distorted finite elements, the locally defined functions for the stresses (Fig. 2) are mapped into the global coordinate system by the Jacobi matrix, evaluated at the center of the element (Fig. 3).

The balanced shape functions for the stresses according to a quadratic approach are deduced from the divergence-free shape functions for linear mixed finite elements developed by Pian [5]. Comparisons have shown, that already a linear approximation of geometry and physics allow analysis of the structural behaviour of thin-walled shells.

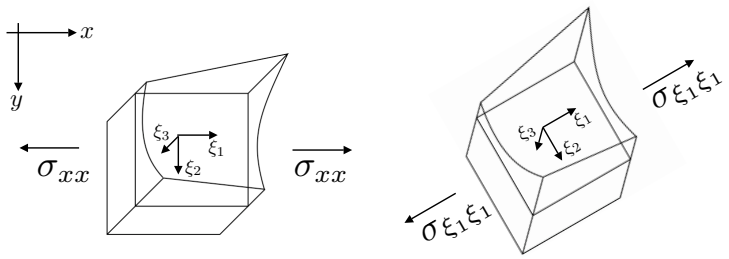

Figure 2: Locally defined ansatz functions

$$\boldsymbol{J} = \begin{bmatrix} \frac{\partial x}{\partial \xi_1} & \frac{\partial y}{\partial \xi_1} & \frac{\partial z}{\partial \xi_1} \\ \frac{\partial x}{\partial \xi_2} & \frac{\partial y}{\partial \xi_2} & \frac{\partial z}{\partial \xi_2} \\ \frac{\partial x}{\partial \xi_3} & \frac{\partial y}{\partial \xi_3} & \frac{\partial z}{\partial \xi_3} \end{bmatrix}$$

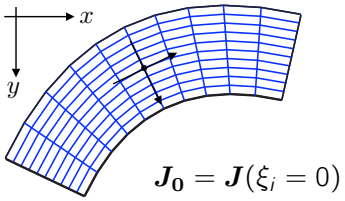

Figure 3: Evaluation of the Jacobian

4.2 Space-time finite element formulation of incompressible fluids

The time-discontinuous, stabilized space-time finite element formulation of the non-Newtonian fluid model within the time slab Q_n reads

$$\int \delta\boldsymbol{v}\,\rho\left(\frac{\partial \boldsymbol{v}}{\partial t} + \boldsymbol{v}\cdot\nabla\boldsymbol{v} - \boldsymbol{b}\right)\,dQ \tag{12}$$

$$+\int \boldsymbol{D}(\delta\boldsymbol{v}) : \phi(p,\boldsymbol{v})\,\boldsymbol{D}(\boldsymbol{v})\,dQ - \int \nabla\cdot\delta\boldsymbol{v}\;p\,dQ \tag{13}$$

$$+\int \delta p\;\nabla\cdot\boldsymbol{v}\,dQ \tag{14}$$

$$+\int \delta\boldsymbol{v}(t_n^+)\cdot\rho\left(\boldsymbol{v}(t_n^+) - \boldsymbol{v}(t_n^-)\right)\,d\Omega \tag{15}$$

$$+\sum_e \int_{Q^e} \tau_M \frac{1}{\rho}\mathcal{L}\left(\delta\boldsymbol{v},\delta p\right)\cdot\left(\mathcal{L}\left(\boldsymbol{v},p\right) - \rho\,\boldsymbol{b}\right)\,dQ \tag{16}$$

$$+\sum_e \int_{Q^e} \tau_C\;\rho\;\nabla\cdot\delta\boldsymbol{v}\;\nabla\cdot\boldsymbol{v}\,dQ = 0, \tag{17}$$

where line (12) and (13) represents the weak form of momentum balance and line (14) the incompressibility constraint of the continuity equation. The velocity jump term of

the time-discontinuous formulation is shown in line (15). The GLS-stabilization of the momentum equation (16) contains the residual of the momentum balance in strong form, defined as

$$\mathcal{L}(\boldsymbol{v}, p) = \rho \left(\frac{\partial \boldsymbol{v}}{\partial t} + \boldsymbol{v} \cdot \nabla \boldsymbol{v} \right) - \nabla \cdot (-p\, \boldsymbol{I} + \phi\, \boldsymbol{D}) \,.$$

The appropriate stabilization parameter

$$\tau_M = \frac{1}{\sqrt{\left(\frac{2}{\Delta t}\right)^2 + \left(\frac{2|\tilde{\boldsymbol{v}}_e|}{h}\right)^2 + \left(\frac{4\,\nu}{h^2}\right)^2}} \tag{18}$$

derived by Tezduyar et al. [7], depends on the characteristic element length h, the time slab width Δt, the kinematic viscosity $\nu = \mu/\rho$ and the velocities $\tilde{\boldsymbol{v}}_e = \boldsymbol{v}_e - \boldsymbol{v}_{N,e}$ between the fluid and its moving mesh. The GLS-stabilization of the continuity equation in line (17), containing the stabilization parameter

$$\tau_C = h\,|\tilde{\boldsymbol{v}}_e|\,\zeta\,(\mathrm{Re}_e) \quad \text{with} \quad \zeta = \begin{cases} \mathrm{Re}_e/3 & \mathrm{Re}_e < 3 \\ 1 & \mathrm{Re}_e \geq 3 \end{cases} \quad \text{and} \quad \mathrm{Re}_e = \frac{|\tilde{\boldsymbol{v}}_e| h}{2\nu} \tag{19}$$

completes the setup of the finite element formulation.

Finite elements with linear and quadratic approximation of the velocities in space have been investigated. The pressure is described linear in both cases, such that the stabilization of the pressure-field is needed only if an equal order (linear) interpolation of the velocities is used. The evolution of the variables $\boldsymbol{v}$ and p in time is described by linear functions independently of the discretization in space.

4.3 Mesh motion approach based on a neo-Hooke pseudo-structure

The continuous fluid-structure mesh with identical orders of approximation for both solid and fluid in space and time automatically yields integral conservation of mass and momentum at the fluid-structure interface.

For large structural displacements updated coordinates have to be found for the mesh nodes inside the fluid domain. In order to avoid overlapping nodes and to reduce distortions of extremely stretched elements a pseudo-elastic continuum following a neo-Hookean material law is used as a mesh-moving scheme.

The elasticity tensor associated to the neo-Hookean material can be specified by

$$\mathbb{C} = \lambda \, \boldsymbol{C}^{-1} \otimes \boldsymbol{C}^{-1} + 2 \left(\mu - \lambda \, \ln(J) \right) \boldsymbol{C}^{-1} \odot \boldsymbol{C}^{-1}, \tag{20}$$

where $\boldsymbol{C} = \boldsymbol{F}^T \boldsymbol{F}$ is the right Cauchy-Green tensor and J^2 its third invariant.

5 LEVEL-SET-METHOD AND EXTENDED SPACE-TIME FINITE ELEMENT METHOD

In order to describe the motion of the free surface of the discharging granular material the level-set-method is applied [8]. The level-set-method implies the solution of the transport equation

$$\mathcal{L}_\phi = \frac{\partial \phi}{\partial t} + \boldsymbol{v} \cdot \nabla \phi = 0 \tag{21}$$

for the distance function ϕ moved by the velocities within the fluid domain. The distance function defines the position of a material point in space and time to an interface separating two domains at zero level ($\phi = 0$). To evaluate the current position of the interface in a space-time slab $Q_n = \Omega_t \times [t_n, t_{n+1}]$, the transport equation is transferred into a time-discontinuous space-time finite element formulation with GLS-stabilization for the convective part of the material derivative as follows

$$\int_Q \delta\phi \left(\frac{\partial \phi}{\partial t} + \boldsymbol{v} \cdot \nabla \phi \right) dQ \tag{22}$$

$$+ \int_\Omega \delta\phi(t_n^+) \left(\phi(t_n^+) - \phi(t_n^-) \right) d\Omega \tag{23}$$

$$+ \sum_e \int_Q \mathcal{L}_\phi(\delta\phi) \, \tau_L \, \mathcal{L}_\phi(\phi) \, dQ = 0. \tag{24}$$

In convection dominated problems the solution of the level-set-equation loses accuracy during the transport process, in particular in the vicinity of inflow-boundaries. To improve the solution of subsequent time-slabs, the level-set-function needs to be reinitialized. Therefore, the fast-marching-method [6] is used as time-efficient algorithm.

Applying the XFEM, kinks in the velocity and jumps in the pressure field between the two fluid domains can be taken into account, extending the approximation of variables u by additional shape functions M in $\mathcal{N}_{\text{ext}}$.

$$u_{\text{ext}}(\mathbf{x}, t) = \sum_{k \in \mathcal{N}_{\text{std}}} N_k(\mathbf{x}, t) \, \hat{u}_k + \sum_{j \in \mathcal{N}_{\text{ext}}} M_j(\mathbf{x}, t) \, \tilde{u}_j \tag{25}$$

In case of linear approximation of the physics in $\mathcal{N}_{\text{std}}$ additional shape functions

$$M_j = N_j(\mathbf{x},t)\,\psi_j^{\text{sgn}}(\mathbf{x},t) \quad \text{with}$$
$$\psi_j^{\text{sgn}}(\mathbf{x},t) = \frac{1}{2}\Big(1 - \text{sgn}\big(\phi(\mathbf{x},t)\big)\cdot\text{sgn}\big(\phi(\mathbf{x}_j,t_j)\big)\Big) \tag{26}$$

based on sgn-enrichment are used to represent discontinuities in the pressure field. On the contrary, the enrichment functions

$$M_j = N_j(\mathbf{x},t)\,R(\mathbf{x},t) \quad \text{with} \quad R(\mathbf{x},t) = \sum_{j\,\in\,\mathcal{N}^{\text{ext}}} |\phi_j| N_j - \Big|\sum_{j\,\in\,\mathcal{N}^{\text{ext}}} \phi_j N_j\Big| \tag{27}$$

for continuous velocities contain a ridge function R for the specification of kinks. In case of quadratic finite elements the pressure approximation is still extended by shape functions based on sgn-enrichment, whereas for the quadratic approximation space of the velocities $\mathcal{N}_{\text{std}}^{\text{quad}}$ linear abs-enrichments $N_j^{\text{lin}}\,\psi_j^{\text{abs}}$ are used following the recommendation of Zilian [9].

For the integration over the fluid domain, XFEM elements have to be subdivided into subelements, where each subelement belongs to a single fluid domain (Fig. 4). With the developed split-algorithm for 4D space-time finite elements, the velocitiy-field of flowing granular material in silos with kernel flow and predefined inner slots can be investigated.

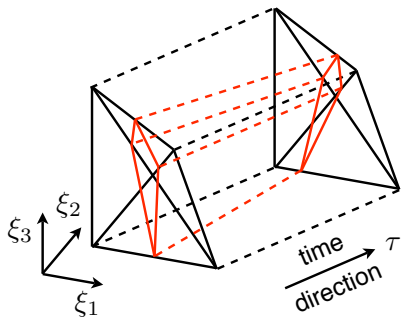

Figure 4: Intersected 4D space-time finite element

6 SOLUTION STRATEGY

To solve the transport equation for the interface the values of the velocities in the fluid domain are needed. On the other hand the enriched approximation space for the physics depends on the position of the interface, which leads to a strongly-coupled problem. To ensure the convergence of the boundary-sensitive problem, while taking the physical and geometrical nonlinearities into account, a staggered solution scheme is used. The outer loop updates the solution of the transport equation with the current velocities, whereas in the inner loop the fluid-structure-interaction problem is solved for a given approximation space by the Newton-Raphson method.

Given the position of the interface separating the two fluid domains, the nonlinear system of discretized model equations for solid (S), fluid (F) and fluid mesh dynamics (M) have to be solved iteratively. To enable a computation in acceptable time steps, the Newton-Raphson method is applied. Therefore the system of algebraic equations has to be differentiated with respect to the unknowns $\hat{\boldsymbol{x}}$. The updated solution to the multi-field problem may be established by computing

$$\hat{\boldsymbol{x}}^{i+1} = \hat{\boldsymbol{x}}^{i} - \left((\boldsymbol{K}|_{\hat{\boldsymbol{x}}^i})^{-1} \, \boldsymbol{r}|_{\hat{\boldsymbol{x}}^i} \right), \tag{28}$$

where $\boldsymbol{r}$ is the right hand side. The structure of the linearized system of equations, assembling matrix $\boldsymbol{K}$, is shown in Fig. 5. In the present case of fluid-structure-interaction the unknowns are given by the physical quantities $\hat{\boldsymbol{v}}$ and $\hat{p}$ and the mesh motion $\hat{\boldsymbol{d}}$ affecting the evaluation of the discretized model equations.

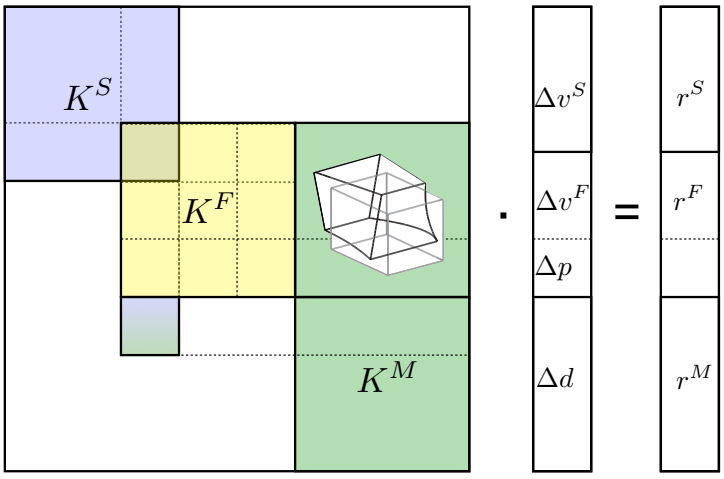

Figure 5: Structure of the strong-coupled linearized system of equations

Velocities as primary variable for both fluid and solid enable a direct coupling that implicates no-slip boundary conditions in between. Slip boundary conditions can be realized by interface elements using Lagrange multipliers to couple the velocities of the two domains at the interface in normal direction $\boldsymbol{n}$. The weak form of the kinematic condition $\boldsymbol{n}\,(\boldsymbol{v}_F - \boldsymbol{v}_S) = 0$ and equilibrium of the normal stress t at the boundary reads

$$\int \delta t\,(\boldsymbol{v}_F - \boldsymbol{v}_S) \cdot \boldsymbol{n}\, dP^D - \int \delta\,(\boldsymbol{v}_F \cdot \boldsymbol{n})\, t\, dP^N + \int \delta\,(\boldsymbol{v}_S \cdot \boldsymbol{n})\, t\, dP^N, \tag{29}$$

leading to the structure of the weak-coupled system of equations shown in Fig. 6.

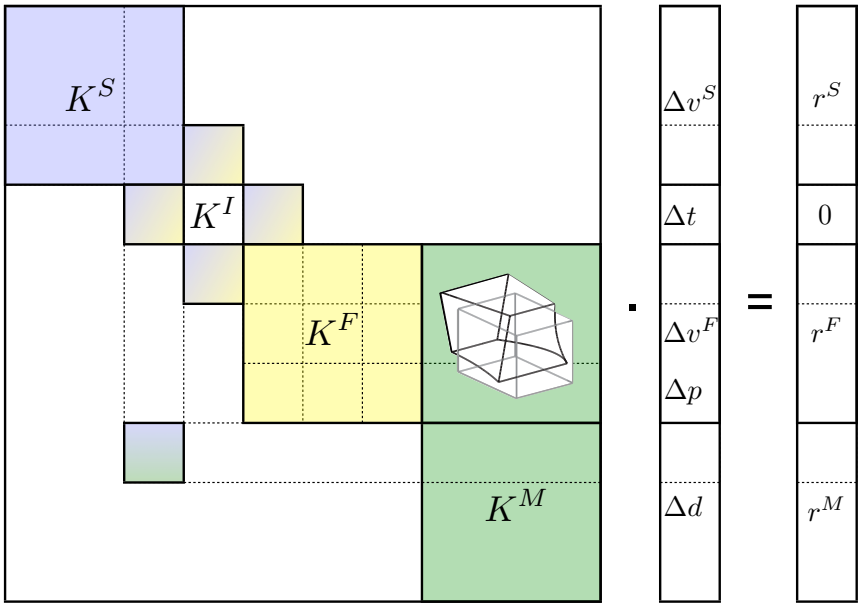

Figure 6: Structure of the weak-coupled linearized system of equations

7 VERIFICATION EXAMPLES

For verification the presented approach is applied to two types of 3D silo discharge. The first example shows a silo with a funnel-shaped discharge zone and a predefined excentric inner slot, streamed by granular material. The dead zone is characterized by nearly inactive cohesive granular material around the inner slot. The velocity of the granular material and flow direction in the inner slot is shown in Fig. 7. Furthermore, the reaction forces around the support and symmetry plane are plotted on the superelevated deformed configuration.

As further example a silo discharge by mass flow caused by gravitation has been computed. The fluid domain inside is connected to the circumferential 3d silo structure by slip

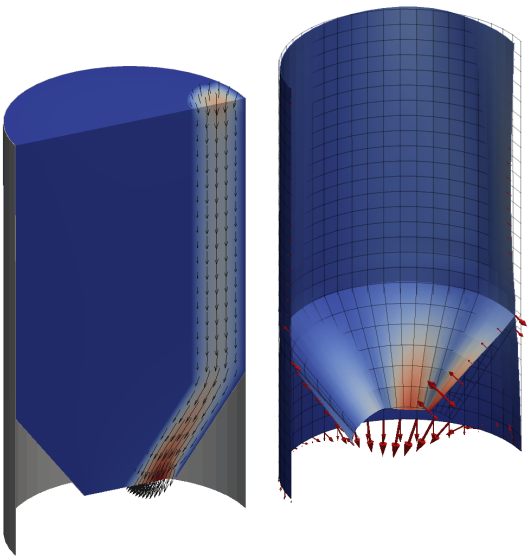

Figure 7: Velocity-field and reaction forces on the deformed configuration

boundary conditions connecting only the velocities of the two domains along the interface in normal direction. An extruded model of the finite element mesh showing the initial state of the filled silo is shown in Fig. 8 on the left. The finite element mesh consists of the shell-structure, the interface and the splitted fluid domain containing a pseudo-solid for mesh movements. The lowering of the free surface between the granular material and air above is depicted in Fig. 8.

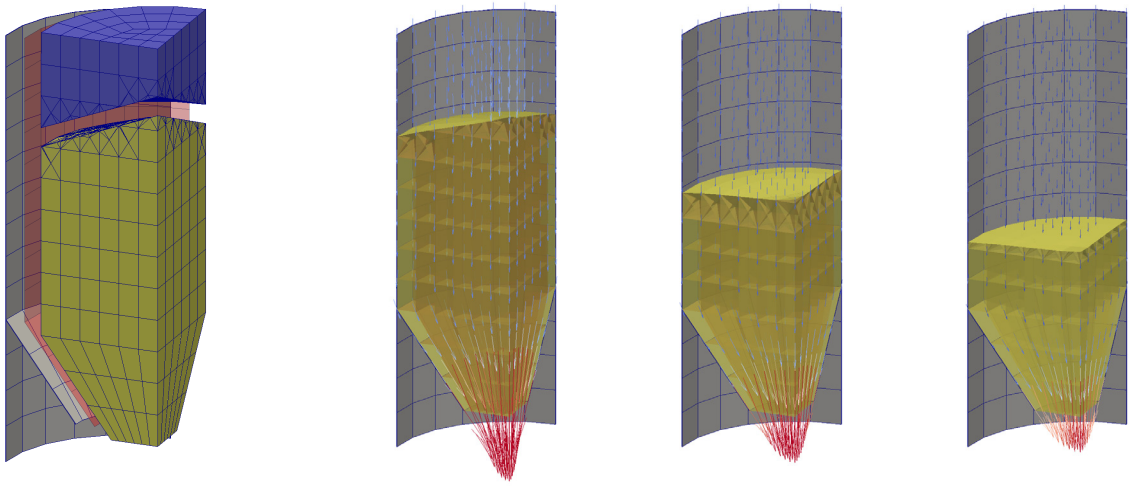

Figure 8: Extruded mesh and lowering of the free surface during emptying

REFERENCES

[1] T. Hughes; G. Hulbert: Space-time finite element methods for elastodynamics: Formulations and error estimates. Computer Methods in Applied Mechanics and Engineering, 66, 3, (1988), 339–363.

[2] B. Hübner; D. Dinkler: A simulatneous solution procedure for strong interactions of generalized Newtonian fluids and viscoelastic solids at large strains, International Journal for Numerical Methods in Engineering 64 (2005) 920–939.

[3] B. Hübner; E. Walhorn; D. Dinkler: A Monolithic Approach to Fluid-Structure Interaction using Space-Time Finite Elements. Computer Methods in Applied Mechanics and Engineering, 193, 23–26, (2004), 2069–2086.

[4] D. Perić; S. Slijepčević: Computational modelling of viscoplastic fluids based on a stabilised finite element method, Engineering Computations, Vol.18 No.3/4 (2001) 577-591.

[5] T. H. H. Pian; K. Sumihara: Rational approach for assumed stress finite elements, Int. J. Numer. Meth. Eng., 20:1685-1695, 1985.

[6] J. A. Sethian; A. Vladimirsky: Fast methods for the Eikonal and related Hamilton-Jacobi equations on unstructured meshes, Proc. Natl. Acad. Sci. USA, 97 (2000) 5699-5703

[7] T. E. Tezduyar; M. Behr: Finite element solution strategies for large-scale flow simulations, Computer Methods in Applied Mechanics and Engineering (112) (1994) 3 – 24.

[8] A. Zilian; A. Legay: The enriched space-time finite element method (EST) for simultaneous solution of fluid-structure interaction, International Journal for Numerical Methods in Engineering 75 (2008) 305–334.

[9] A. Zilian; A. Legay: Enriched space-time finite elements for fluid-thin structure interaction, European Journal of Computational Mechanics, 17:725-736, 2008.